Supporting Information

A multifunctional polymer electrolyte enables high-voltage lithium metal battery ultra-long cycle-life

Tiantian Dong,[†][a] Jianjun Zhang,[†][b] [c] Gaojie Xu,[b] Jingchao Chai,[b] [c] Huiping Du,[b] [c] Longlong Wang,[b] [c] Huijie Wen,[b] Xiao Zang,[a] Aobing Du,[b] [c] Qingming Jia,*[a] Xinhong Zhou,* [d] Guanglei Cui *[b]

[†] These authors contributed equally to this work.

[a]School of Chemical Engineering, Kunming University of Science and Technology, Kunming 650500, P. R. China.

[b]Qingdao Industrial Energy Storage Research Institute, Qingdao Institute of Bioenergy and Bioprocess Technology, Chinese Academy of Sciences, No. 189 Songling Road, 266101, Qingdao, China.

[c]University of Chinese Academy of Sciences, No.19A Yuquan Road, 100049, Beijing, China.

[d]College of Chemistry and Molecular Engineering, Qingdao University of Science and Technology, Qingdao, 266042, China.

*Email: jiaqm411@163.com, zxhhx2008@163.com, cuigl@qibebt.ac.cn

Table of Contents

Experimental section

1. Preparation of electrolytes

1.0 g poly (methyl vinyl ether-alt-maleic anhydride) powder (abbreviated as "P(MVE-MA) ") was dissolved into 10 g acetonitrile and stirred for 5 hrs. Then, the obtained solution was coated on modified bacterial cellulose. The modified bacterial cellulose was prepared according to the method of previous literature. [1,2] Subsequently, the resultant P(MVE-MA) membrane was dried at 60 ^{o}C for 48 hrs. Last, above P(MVE-MA) membrane was saturated in propylene carbonate (PC) containing 1 M lithium difluoro(oxalato) borate (LiODFB) for 24 hrs and the gel polymer electrolyte (hereafter abbreviated as "PMM-CPE") was obtained. For the electrolyte, the weight ratio of PC/LiODFB to P(MVE-MA) was 3:7. The fabrication process of PMM-CPE was vividly shown in Figure S1a.

2. Materials

Poly (methyl vinyl ether-alt-maleic anhydride), Mw=1,080,000) used in this work was purchased from Sigma-Aldrich. Lithium oxalyldifluroborate (LiODFB) was supplied by Jiangsu Guotai Super Power New Materials Co., Ltd. Propylene carbonate (PC) was supplied by Suzhou Qianmin Chemistry Co., Ltd. 1 M $LiPF_6$-EC/DMC (1/1,v/v) was obtained from Shenzhen Capchem Technology Co., Ltd. PP separator (Celgard 2500) was received from Celgard Co. (USA). Bacterial cellulose was purchased from Hainan Guangyu company. Acetonitrile was commercially available.

3.Characterization

To tested the uptake of different electrolytes, the P(MVE-MA) membrane and the PP separator were immersed in the corresponding liquid electrolyte solution for 24 h,

respectively. Subsequently, the excess solution was slightly absorbed using filter paper. The uptake was obtained by measured the weight before and after soaking in liquid electrolyte. Electrolyte uptake = (Wf −Wi)/Wi ×100%, where Wi and Wf were the weight of the P(MVE-MA) membrane or the PP separator before and after soaking in the corresponding liquid electrolyte, respectively. The morphology and energy dispersive X-ray spectroscopy of the samples were obtained by a field emission scanning electron microscope testing (Hitachi S-4800 at 3 kV). ESCALab220i-XL spectrometer was used to investigate the X-Ray photoelectron spectrometer (XPS) of samples at ambient temperature. The stress-strain curves were tested by an Inston-3300 universal testing machine (USA) at a stretching speed of 10 mm min^{-1} with a rectangular sample of 1 cm wide and 8 cm long. The gage length was 6 cm with both ends of samples were encased for 1 cm length and stretched until the samples was broken. The surface morphology and Young's modulus of PP separator and bacterium cellulose were measured by Atomic force microscopy (Multimode 8, AFM) with PFT-QNM mode. The surface morphologies of the cycled $LiCoO_2$ electrodes were characterized by using high resolution TEM (Tecnia G20, FEI). The crystal structures of all samples were identified by X-ray diffraction (XRD, Ultima IV) in the 2θ angular. The amount of Co ions were measured using inductively coupled plasma-optical emission spectrometer (ICP-OES, Optima 8300).

4. Electrochemical evaluation

Ionic conductivity of the samples was tested via the EIS measure over the temperature ranging from 25 °C to 80 °C. The frequency ranges from 100 mHz to 1 MHz with an AC amplitude of 10 mV. Ionic conductivity was calculated by using following equation $\sigma = \frac{L}{SR}$, where R represents the bulk resistance of polymer

electrode(R was determined from the impedance spectrum), L and S are the thickness and area of the samples. Electrochemical stability of the samples were determined by a linear sweep voltammetry (LSV) experiment performed on a working electrode of stainless steel as a counter and a reference electrode of lithium metal at a scan rate of 1 mV s^{-1} over the range of 0 - 6 V at 25 ºC. The lithium ion transfer number was measured the initial resistance by AC impedance in the frequency ranging from 1 Hz to 1 MHz, subsequently, a DC potential of 10 mV of PMM-CPE and 5 mV of LE using PP separator were tested until a steady state was reached, respectively. In the end, the resistance was tested again. The lithium ion transfer numbers were calculated using Bruce-Vincent-Evans equation $t_{Li+} = \frac{I_{ss}}{I_o} \cdot \frac{(V - I_o R_o)}{(V - I_{ss} R_{ss})}$, where V is the applied polarization voltage, I_o and R_o are the initial current and the initial interfacial resistance before polarization, respectively, I_{ss} and R_{ss} are the steady-state current and the steady-state interfacial resistance after polarization for 10000 s, respectively. For cell performance tests, the $LiCoO_2$ cathode was prepared in a conventional cast-coating method, by mixing 80 wt.% $LiCoO_2$, 10 wt.% acetylene black, and 10 wt.% PVdF. Areal density of obtained $LiCoO_2$ cathode was 1 mg cm^{-2}. Rate capability and cycle life of $LiCoO_2$/Li battery were conducted on LAND testing system (Wuhan LAND electronics Co., Ltd.) in the voltage range of 2.75 V - 4.45 V at 25 ºC and 60 ºC, respectively. The C rates in all of the electrochemical measurements are defined based on 1 C = 170 mA g^{-1}.

5. Calculation Methods

All quantum chemical calculations were performed with B3LYP level and 6-311G

(d,p) basis set using the framework of Gaussian 09 program package. The structural optimization was determined by minimizing the energy without imposing molecular symmetry constraints based on density functional theory. To simplify our calculation, long P(MVE-MA) chains were replaced by three repeat units group, and this simplified method had been successfully reported.[3,4] The HOMO-LUMO analysis has been performed to explain the redox ability for PC or P(MVE-MA). And the absorbing energy (E_b) can be given as $E_b=E_{total}-(E_{DFOB}+Ed)$, where E_{toatl} is total energy the adsorbed system, E_{DFOB} is $DFOB^-$ energy, Ed is energy of P(MVE-MA).

Supplementary Figures and discussions

Figure S1. a) Typical SEM image of P(MVE-MA) membrane and the corresponding elemental mapping images of b) C and c) O.

The surface of P(MVE-MA) membrane was smooth and all of the elements C) and O) were uniformly dispersed on the surface of membrane, indicating the successful preparation of P(MVE-MA) membrane.

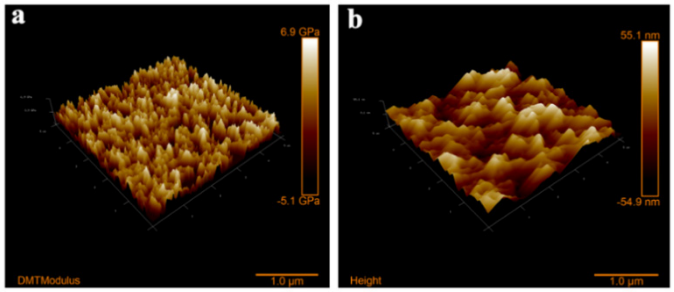

Figure S2. a) AFM image of P(MVE-MA) membrane and b) the corresponding Young's modulus mapping image.

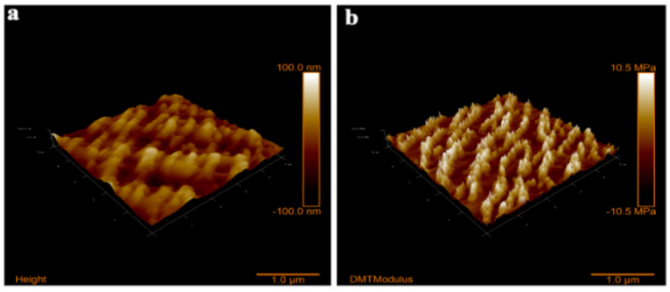

Figure S3. a) AFM image of PP separator and b) the corresponding Young's modulus mapping image.

As shown in **Figure S3**, the Young's modulus of PP separator was only10.5 MPa, which was much lower than that (6.9 GPa) of P(MVE-MA) membrane (**Figure S2**).

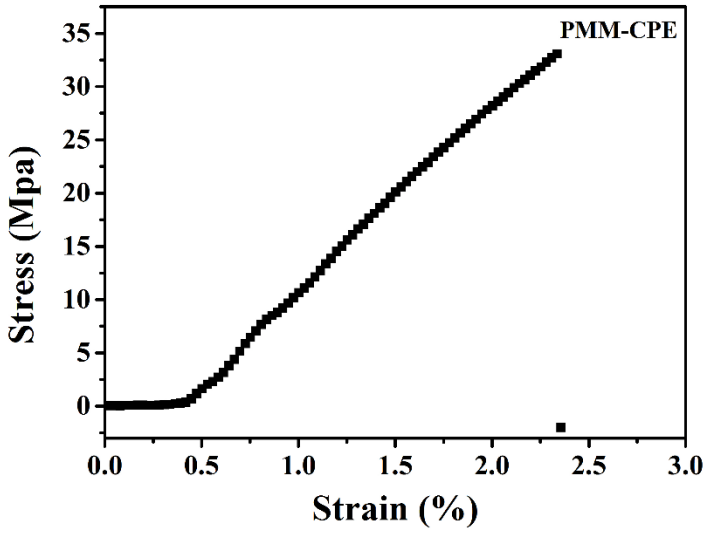

Figure S4. Stress-strain curves of PMM-CPE.

As shown in **Figure S4**, PMM-CPE (P(MVE-MA) membrane uptake liquid electrolyte) presented satisfactory mechanical strength (up to 32 Mpa) owing to the existence of bacterial cellulose.

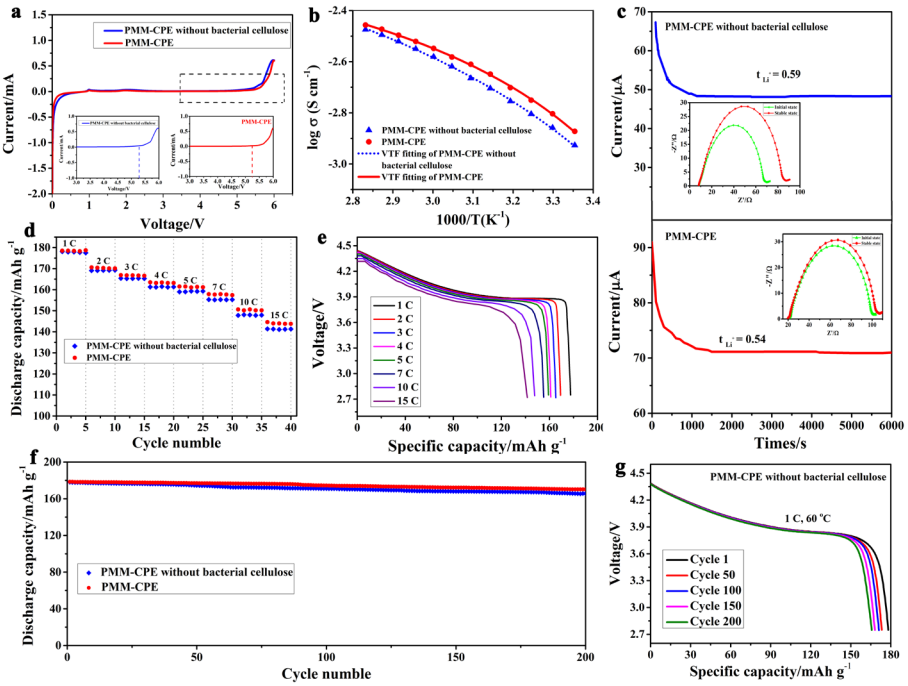

Figure S5. a) Linear sweep voltammetry comparison of PMM-CPE without bacterial cellulose and PMM-CPE. b) Temperature dependent of ionic conductivity of PMM-CPE without bacterial cellulose and PMM-CPE. c) Current-time curve following a DC polarization of PMM-CPE without bacterial cellulose and PMM-CPE with 0.01 V. The insets are AC impedance spectra of two electrolytes, respectively. d) Rate capability of 4.45 V-class $LiCoO_2$/Li cell using PMM-CPE without bacterial cellulose and PMM-CPE at 60 ºC. e) Discharge voltage curves of 4.45 V-class $LiCoO_2$/Li cell using PMM-CPE without bacterial cellulose at varied current rates. f) Cycle performance (1 C) of 4.45 V-class $LiCoO_2$/Li cell using PMM-CPE without bacterial cellulose and PMM-CPE at 60 ºC. g) The corresponding discharge voltage curves of 1^{st}, 50^{th}, 100^{th}, 150^{th} and 200^{th} cycle of $LiCoO_2$/Li cell using PMM-CPE without bacterial cellulose at 60 ºC. As can be seen from Figure S5a, there was no obvious oxidative decomposition of PMM-CPE without bacterial cellulose until 5.2 V versus Li/Li+, which was similar to PMM-CPE. And from Figure S5b, PMM-CPE delivered higher ionic conductivity than that of PMM-CPE without bacterial cellulose from 25 ºC to 80 ºC. The liquid uptake of PMM-CPE was higher than that of PMM-CPE without bacterial cellulose owing to the existence of bacterial cellulose. Figure S5c presented the comparison of lithium ion transference number between PMM-CPE without bacterial cellulose and PMM-CPE. From Bruce-Vincent-Evans equation, we could easily get the tLi+ of PMM-CPE without bacterial cellulose was 0.59, which was higher than PMM-CPE (0.54). The rate capability of 4.45 V-class LiCoO2/Li cells using PMM-CPE without bacterial cellulose and PMM-CPE at 60 oC were vividly shown in Figure S5d. As shown in Figure S5d, the LiCoO2/PMM-CPE/ Li cell could maintained a relatively large discharge capacity with increasing the current rate from 1 C to 15 C owing to PMM-CPE delivered higher

ionic conductivity than that of PMM-CPE without bacterial cellulose from 25 °C to 80 °C. And from Figure S5e, neither abnormal nor unstable discharge profiles were observed in the $LiCoO_2$/PMM-CPE without bacterial cellulose/Li cell. Moreover, from Figure S5f (cycle performance), compared with PMM-CPE, there was no obvious change in a limited cycles using PMM-CPE without bacterial cellulose.

Table S1. The fitting results, ionic conductivity and electrolyte uptake of $LiPF_6$/EC-DMC electrolyte, LiODFB/PC electrolyte and PMM-CPE.

	A ($S\ cm^{-1}\ K^{-1/2}$)	E_a (eV)	Conductivity ($S\ cm^{-1}$) (25 °C)	Conductivity ($S\ cm^{-1}$) (60 °C)	Electrolyte uptake (wt.%)
$LiPF_6$/EC-DMC electrolyte (with PP separator)	0.027	0.078	1.46×10^{-3}	2.03×10^{-3}	120
LiODFB/PC electrolyte (with PP separator)	0.012	0.079	5.51×10^{-4}	8.95×10^{-4}	110
PMM-CPE	0.0094	0.009	1.34×10^{-3}	2.83×10^{-3}	650

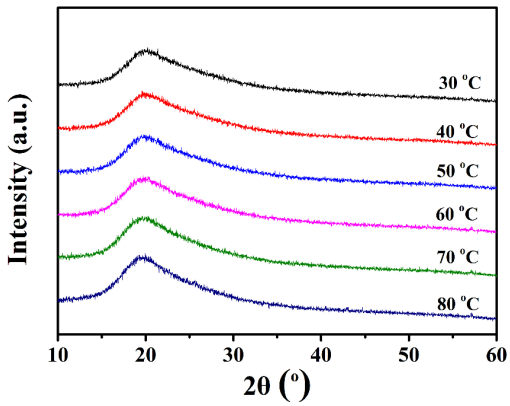

Figure S6. XRD patterns of PMM-CPE at 30 °C, 40 °C, 50 °C, 60 °C, 70 °C and 80 °C.

X-ray diffractogram measurements were made to examine crystallinity of PMM-CPE from 30 to 80 °C in **Figure S6**. As shown in Figure S6, there was no sharp crystalline peak, indicating PMM-CPE was a typical amorphous phase from 30 to 80 °C.

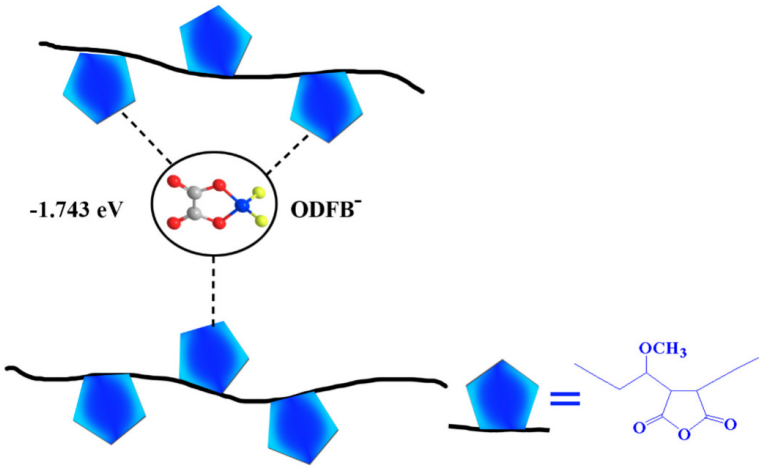

Figure S7. Schematic diagram of interaction energy of P(MVE-MA) and $ODFB^-$.

As shown in Figure S7, adsorption energy for $ODFB^-$ of P(MVE-MA) was -1.743 eV, indicating there was some kind of interaction between P(MVE-MA) and $DFOB^-$.

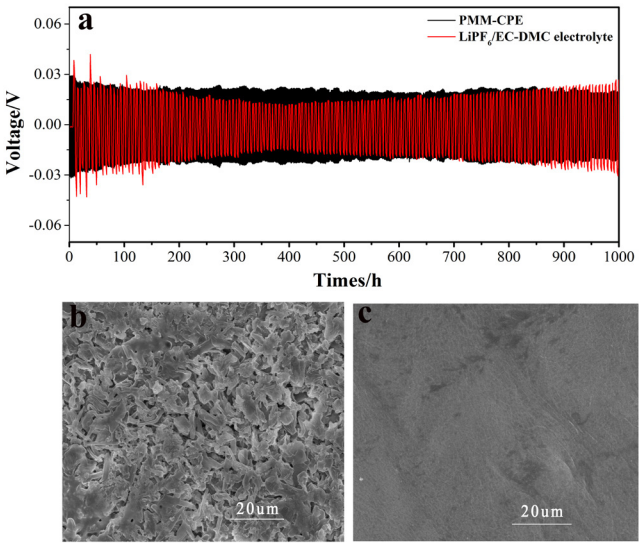

Figure S8. a) Comparison of lithium plating/stripping experiment for symmetric Li/Li cells with $LiPF_6$/EC-DMC electrolyte and PMM-CPE at a current density of 0.1 mA cm^{-2} (0.5 hour in each half cycle). Typical SEM images of Li metal electrode in Li/Li

cells after 1000 hrs stripping/plating using b) $LiPF_6$/EC-DMC electrolyte and c) PMM-CPE.

As shown in **Figure S8**a, the symmetric Li/PMM-CPE/Li cells exhibited steady lithium plating/striping at the current density of 0.1 mA cm^{-2}. After cycling for 1000 hrs polarization, no sign of short circuit was observed. In addition, the surface of lithium anode (Figure S8c) was smooth and flat, indicating PMM-CPE could suppress the growth of dendritic Li effectively. On the contrary, the galvanostatic discharge/charge voltage curve (Figure S8a) of Li/$LiPF_6$/EC-DMC/Li cell was unstable and suffered from severe polarization. Moreover, the surface of metallic Li was not smooth and there existed an obviously lithium dendrite after cycling for 1000 hrs polarization (Figure S8b).

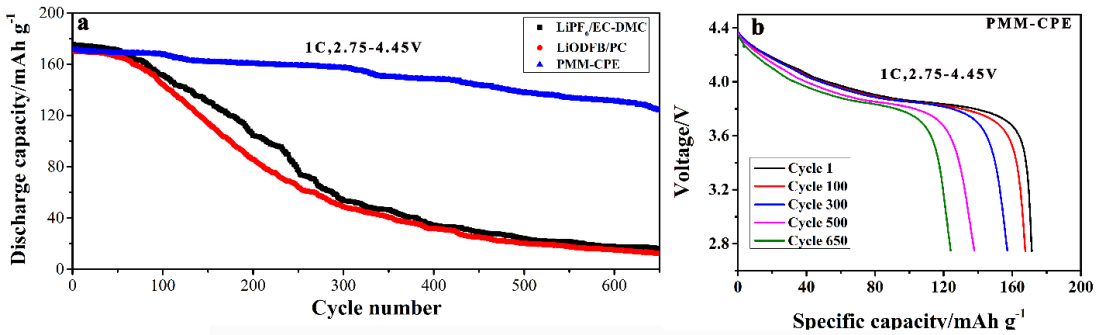

Figure S9. a) Long-term cycle performance (1 C) of 4.45 V-class $LiCoO_2$/Li cell using $LiPF_6$/EC-DMC electrolyte, LiODFB/PC electrolyte and PMM-CPE at 25 ºC. b) The corresponding discharge voltage curves of 1st, 100th, 300th, 500th and 650th cycle of $LiCoO_2$/Li cell using PMM-CPE at 25 ºC.

Cycle performance of $LiCoO_2$/Li cells using $LiPF_6$/EC-DMC electrolyte, LiODFB/PC electrolyte and PMM-CPE at 25 ºC were also presented in **Figure S9.** As shown in Figure S9, the capacity decay of $LiCoO_2$/Li cells using $LiPF_6$/EC-DMC electrolyte and LiODFB/PC electrolyte was severe. In contrast, the capacity retention

of $LiCoO_2$/Li cell using PMM-CPE was 73 % after 650 cycles, which was much better than those of above-mentioned electrolyte system.

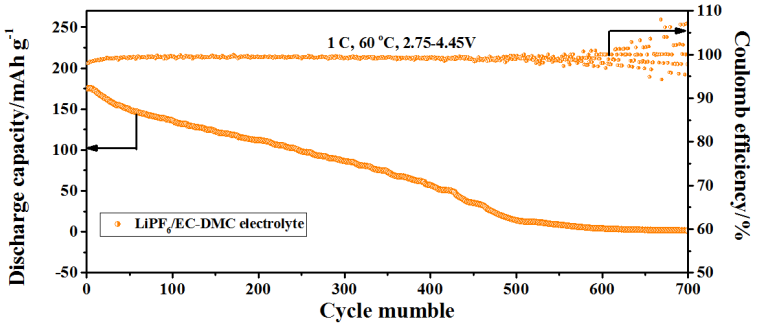

Figure S10. Long-term cycle performance (1 C) of 4.45 V-class $LiCoO_2$/Li cell using $LiPF_6$/EC-DMC electrolyte at 60 °C.

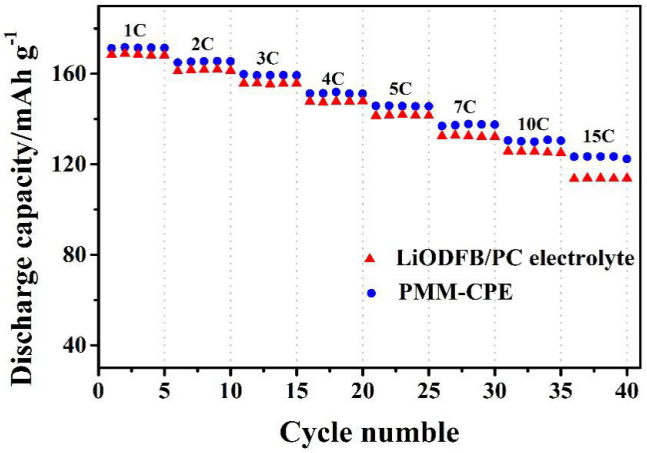

Figure S11. Rate capability of 4.45 V-class $LiCoO_2$/Li cell using LiODFB/PC electrolyte and PMM-CPE at 25 °C.

The rate capability of 4.45 V-class $LiCoO_2$/Li cells using PMM-CPE at 25 °C was vividly showed in **Figure S11**. Obviously, the specific discharge capacity of the cell using PMM-CPE was 171 mAh g^{-1} at 1 C. More interestingly, the discharge capacity still reached 128 mAh g^{-1} even at ultrahigh rate of 15 C. The discharge capacity was higher than 4.45 V-class $LiCoO_2$/Li cell using f LiODFB/PC electrolyte.

Table S2. Cycle performance comparison of $LiCoO_2$ metal batteries.

Authors	Battery configuration	Approach	Cycle performance	Temperature	Voltage range
Cui et al.[5]	$LiCoO_2$/Li	PVCA- SPE **(SPE)**	84 % after 150 cycles at 0.1 C	50 ºC	2.5 V-4.3 V
Matsui et al.[6]	$LiCoO_2$/Li	P(EO/MEEGE/AGE)-SPE **(SPE)**	63 % after 200 cycles at 0.2 C	60 ºC	3.0 V-4.2 V
Zhang et al.[7]	$LiCoO_2$/Li	0.8 M $LiPF_6$ in EC:DEC:NEO solvent with VC +LiODFB **(electrolyte additive)**	97 % after 50 cycles at 0.2 C	25 ºC	3.0 V-4.4 V
Kim et al.[8]	$LiCoO_2$/Li	80 % LLZO,19 % $Py_{14}TFSI$,1 % LiTFSI (**hybrid solid electrolyte)**	93 % after 150 cycles at 0.1 C	25 ºC	3.0 V-4.3 V
Qin et al.[9]	$LiCoO_2$/Li	1 M $LiPF_6$/TESM2 electrolytes with 1 % (volume ratio) VC additive **(electrolyte additive)**	90 % after 80 cycles at 0.2 C	25 ºC	3.0 V-4.35 V
Yang et al.[10]	$LiCoO_2$/Li	5 % suberonitrile as additive with 0.1 M LiBOB in 1 M EC-DMC/$LiPF_6$ solutions **(electrolyte additive)**	62.3 % after 500 cycles at 140 mAg^{-1}	30 ºC	3.0 V-4. 5 V
Our work	$LiCoO_2$/Li	PMM-CPE **(GPE)**	85 % after 700 cycles at 1 C	60 ºC	2.75 V-4.45V
Our work	$LiCoO_2$/Li	PMM-CPE **(GPE)**	73 % after 650 cycles at 1 C	25 ºC	2.75 V-4.45V

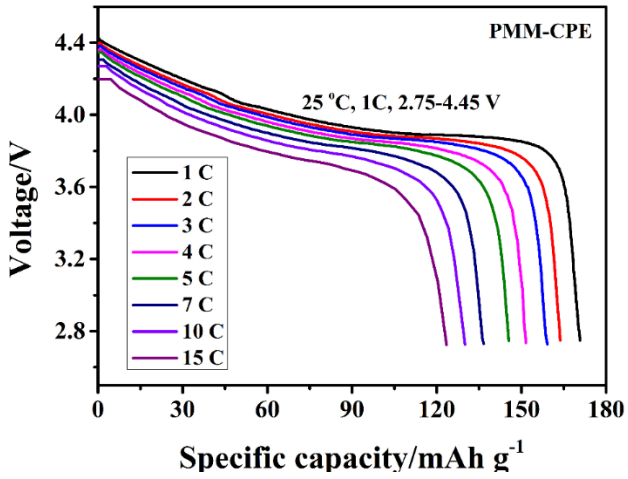

Figure S12. Discharge voltage curves of 4.45 V-class $LiCoO_2$/Li cell using PMM-CPE at varied current rates (25 ºC).

From **Figure S12**, neither abnormal nor unstable discharge profiles were observed in the $LiCoO_2$/PMM-CPE/Li cell at 25 ºC.

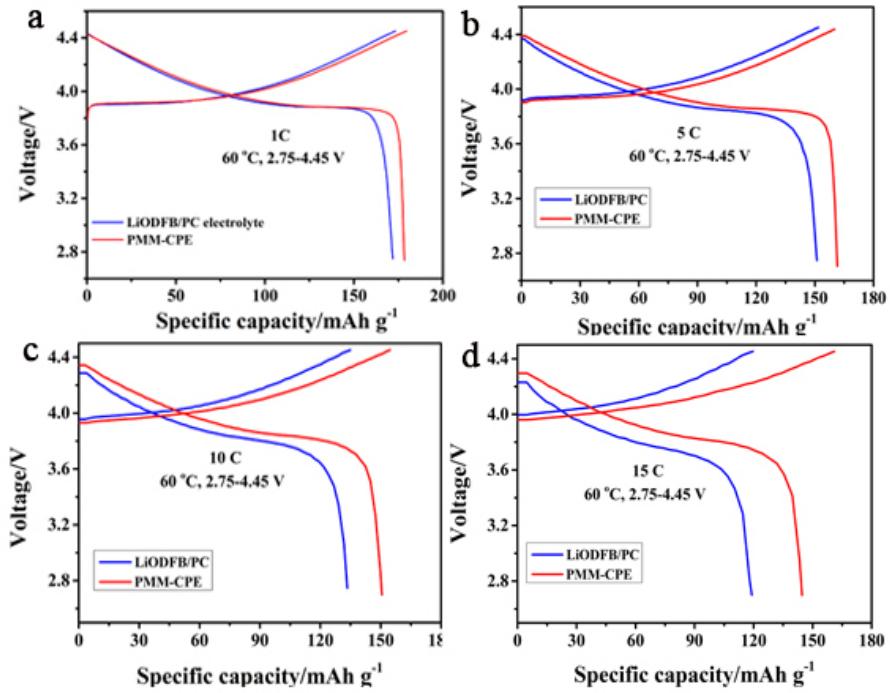

Figure S13. The charging/discharging profiles of the LiODFB/PC electrolyte and PMM-CPE at a) 1 C, b) 5 C, c) 10 C and d) 20 C.

From **Figure S13,** the charging/discharging voltage polarization of $LiCoO_2$/PMM-CPE/Li cell was lower than $LiCoO_2$/LiODFB/PC/Li cell at 60 ºC, indicated the cycle performance of $LiCoO_2$/Li cell using PMM-CPE was superior than LiODFB/PC electrolyte.

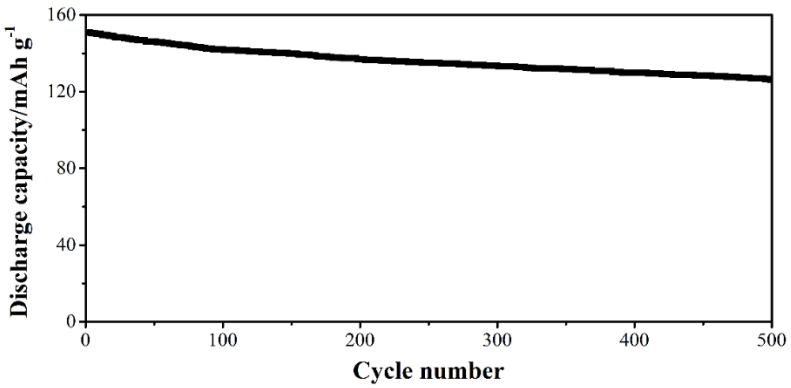

Figure S14. Cycle performance (10 C) of 4.45V-class $LiCoO_2$/Li cell using PMM-CPE at the elevated temperature of 60 ºC.

4.45V-class $LiCoO_2$/Li cell using PMM-CPE delivered excellent cycling stability even at high current. The capacity retention (10 C) of $LiCoO_2$/PMM-CPE/Li cell was 83 % after 500 cycles at 60 ºC .

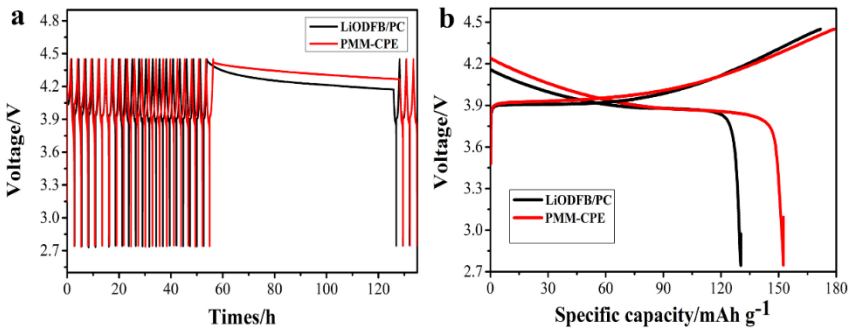

Figure S15. a) Voltage-time curve for self-discharge after 20 cycles and b) charge/discharge curve at 21 cycle of $LiCoO_2$/Li cells using LiODFB/PC electrolyte and PMM-CPE.

Figure S15 displayed the self-discharge phenomenon of $LiCoO_2$/Li cells using LiODFB/PC electrolyte and PMM-CPE. As shown in Figure S15, the cell using PMM-CPE presented slight self-discharge phenomena than that of LiODFB/PC

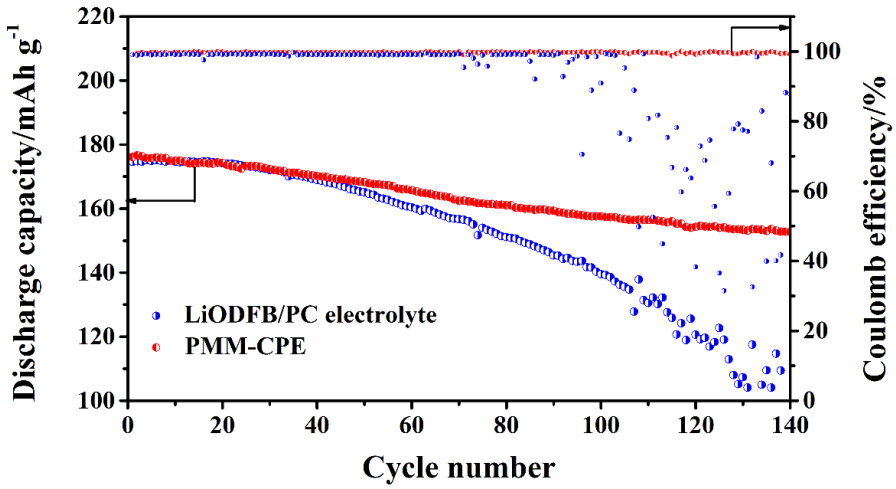

Figure S16. Cycle performance comparision (1 C) of 4.45 V-class $LiCoO_2$/Li cell using LiODFB/PC electrolyte and PMM-CPE at 60 ºC (areal density was 5 mg/cm^2).

As shown in the following **Figure S16**, the $LiCoO_2$/Li cell using PMM-CPE demonstrated an excellent discharge capacity retention of 87 % (153 mAh g^{-1}) of the initial capacity (176 mAh g^{-1}) after 140 cycles. However, the capacity retention of $LiCoO_2$/Li cells using LiODFB/PC electrolyte was only 52 %, which was much lower than that of PMM-CPE. Furthermore, the $LiCoO_2$/Li cell with PMM-CPE demonstrated a higher and more stable Coulombic efficiency (CE) than LiODFB/PC electrolyte.

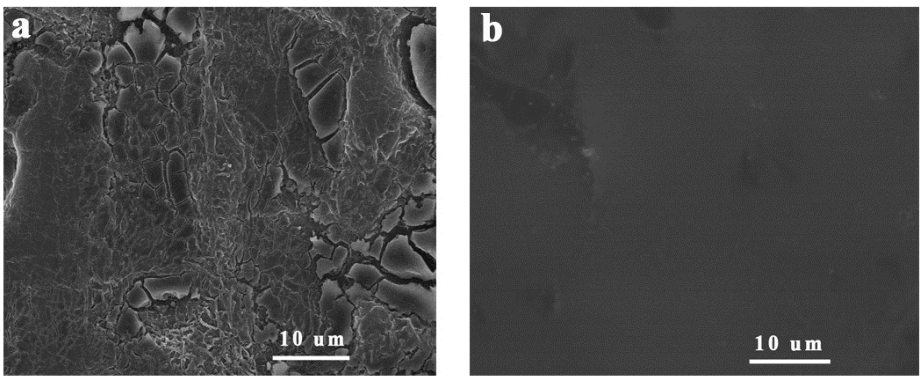

Figure S17. Typical SEM images of Li metal electrode in $LiCoO_2$/Li cells after 140 hrs using a) LiODFB/PC electrolyte and b) PMM-CPE.

We also tested typical SEM images of Li metal in $LiCoO_2$/Li cells (with loading of 5 mg/cm^2) after 140 hrs using LiODFB/PC electrolyte and PMM-CPE, respectively. As shown in the following **Figure S17**, the surface of Li metal anode in $LiCoO_2$/Li battery using LiODFB/PC electrolyte delivered a rough surface morphology with obvious cracks after 140 cycles. In a sharp contrast, the Li metal anode in $LiCoO_2$/ Li battery using PMM-CPE exhibited a smooth and compact surface without obvious lithium dendrites even after 140 cycles.

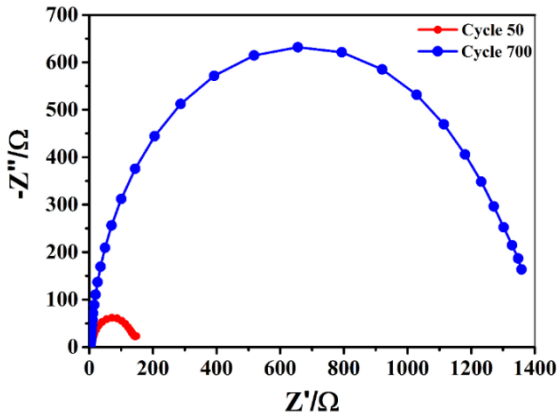

Figure S18. EISs of 4.45 V-class $LiCoO_2$/Li cell using $LiPF_6$/EC-DMC electrolyte after 50 cylces and 700 cycles at 1 C (60 ºC).

As can be seen in **Figure S18**, the interfacial resistance of the cell using $LiPF_6$/ EC-DMC electrolyte increased to a certain extent during the first 700 cycles.

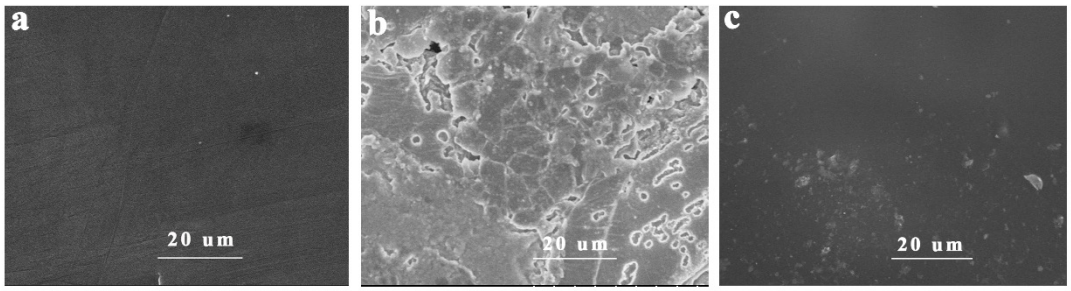

Figure S19. Typical SEM images of Li metal anode. The morphology of Li anode a) pristine, b) disassembled from $LiCoO_2$/Li battery using LiODFB/PC electrolyte after 700 cycles and c) disassembled from $LiCoO_2$/Li battery using PMM-CPE after 700 cycles.

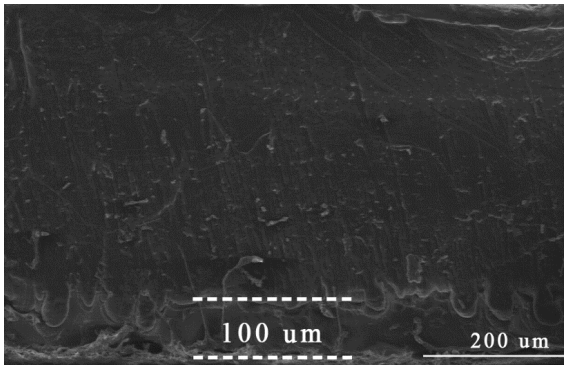

Figure S20. Side-view SEM image of Li metal anode disassembled from $LiCoO_2$/Li battery using PMM-CPE after 700 cycles.

As shown in **Figure S19**a, the surface of fresh lithium anode was smooth and dense. After 700 cycles, the surface of Li metal anode in $LiCoO_2$/Li battery using LiODFB/PC electrolyte exhibited a severe corrosion and a moss-like dendrite structure (Figure S19b). In a sharp contrast, the Li metal anode in $LiCoO_2$/Li battery using PMM-CPE displayed a smooth surface without obvious dendrite structure (Figure S19c). In addition, Li metal also exhibited a smooth and compact interface without dendrite structure with a thickness about 400 μm (**Figure S20**).

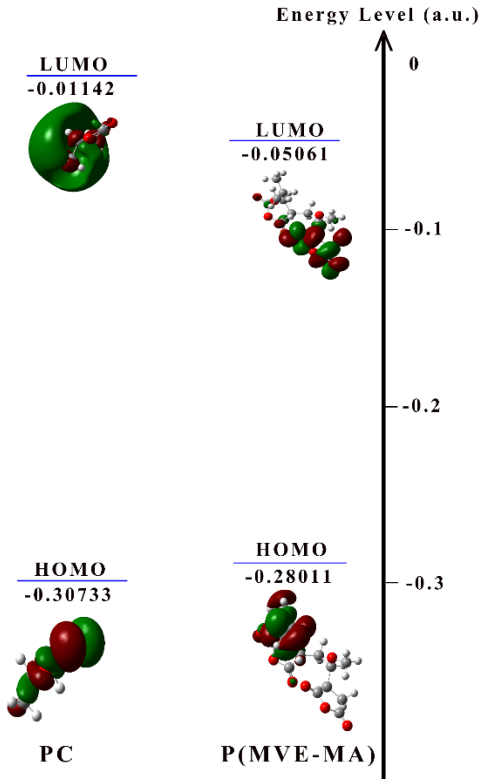

Figure S21. HOMO-LUMO of PC and P(MVE-MA) and the correlated Energy-Level diagram.

The highest occupied molecular orbital (HOMO) energy level and the lowest unoccupied molecular orbital (LUMO) energy level can be calculated. As shown in **Figure S21**, the obtained LUMO energy was -0.05061 a.u. for P(MVE-MA) , which was lower than PC (-0.01142 a.u.). In addition, the HOMO energy of P(MVE-MA) was -0.28011 a.u., which was higher than PC (-0.30733 a.u.). Based on above mentioned analysis, P(MVE-MA) not only easy accepted electrons but also easy lost electrons than PC. In other words, P(MVE-MA) not only was preferentially to be reduced in Li metal but also was preferentially oxidized at $LiCoO_2$ cathode side. Therefore, combined with LUMO and HOMO results, it was inferred that P(MVE-MA) not only was preferentially reduced at Li metal anode side to form a new SEI layer constituent but also was preferentially oxidized at $LiCoO_2$ cathode side to a new CEI layer constituent.

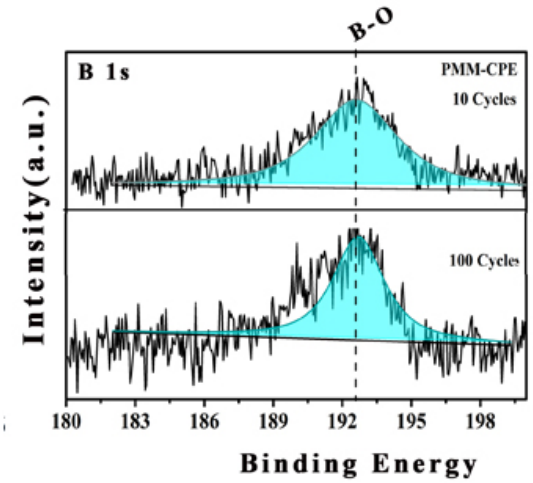

Figure S22. XPS spectra of Li metal anode disassembled from $LiCoO_2$/Li batteries using PMM-CPE after 10 cycles and 100 cycles of B 1s.

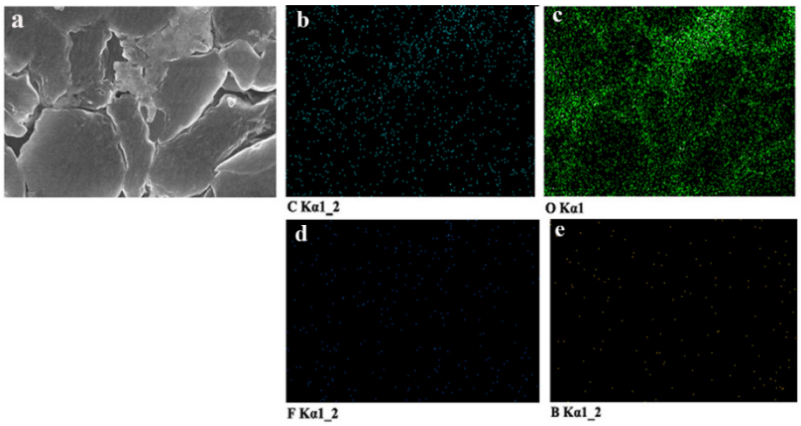

Figure S23. a) Typical SEM image of Li anode disassembled from $LiCoO_2$/Li battery using LiODFB/PC electrolyte after 700 cycles , and corresponding elemental mapping images of b) C, c) O, d) Fluorine (F) and e) Boron (B).

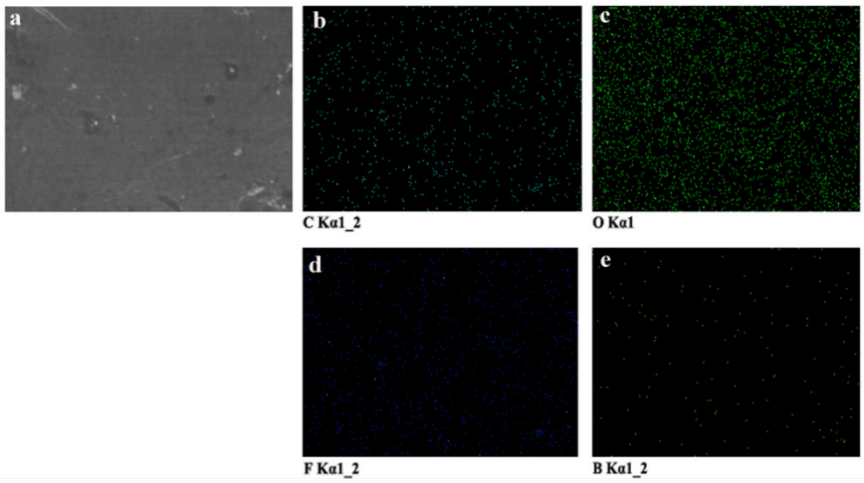

Figure S24. a) Typical SEM image of Li anode disassembled from $LiCoO_2$/Li battery using PMM-CPE after 700 cycles , and corresponding elemental mapping images of b) C, c) O, d) Fluorine (F) and e) Boron (B).

From the data of **Figure S24**, all of the elements were uniformly distributed on the Li metal surface when using PMM-CPE, indicating that the composition of SEI layer distributed uniformly. However, the elements on the Li metal using LiODFB/ PC were non-uniform (**Figure S23**).

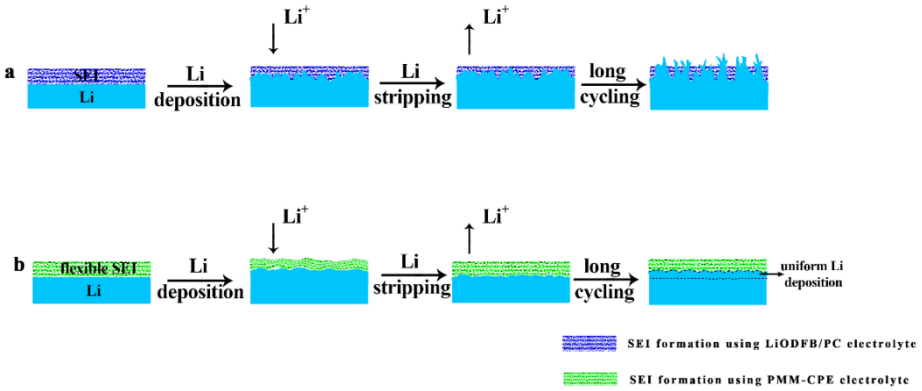

Figure S25. Schematic diagram of Li deposition on the surface using a) LiODFB/ PC electrolyte and b) PMM-CPE during SEI formation and cycling.

As schematically summarized in **Figure S25**, Li deposition on the surface of two different samples were illustrated. From Figure S25a, Li metal contacting with

LiODFB/PC electrolyte instantly formed a SEI layer on the Li surface. After long-term cycling, the Li deposition nonuniformity and lead to severe lithium dendrites. In contrast, P(MVE-MA) participated in the formation of stable and flexible SEI film on Li metal anode (Figure 4c-d and Figure S22). The resultant SEI layer will be embossed during the Li deposition and then recover after Li stripping owing to the contribution of SEI film flexibility. In addition, even in the worst-case scenario (SEI film breakdown after long-term cycling and Li dendrite formed), the ultra-strong bacterial cellulose with high young modulus (6.9 GPa) will further suppress the growth of Li dendrite. From above-mentioned discussion, PMM-CPE not only buffered the volume change of Li metal anode but also suppressed Li dendrite growth owing to synergetic contribution of bacterial cellulose and P(MVE-MA).

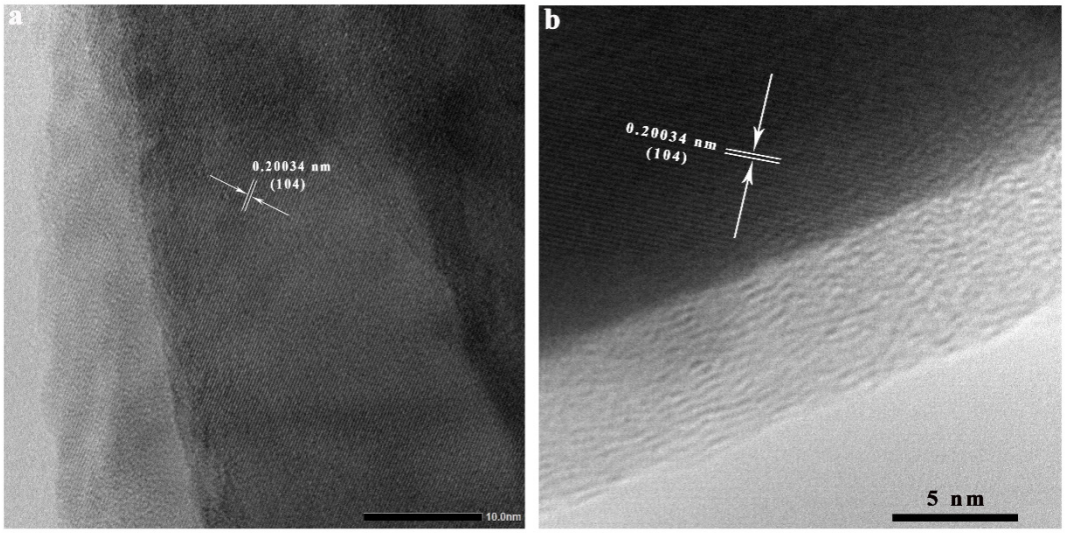

Figure S26. High resolution transmission electron microscopy (HR-TEM) images a) pristine $LiCoO_2$ electrode, and b) cycled $LiCoO_2$ electrodes disassembled from $LiCoO_2$/PMM-CPE/Li battery after 100 cycles at 60 ° C.

As shown in Figure S26a, the pristine $LiCoO_2$ electrode depicted clearly lattice friges and corresponding to the (104) facet. In addition, the $LiCoO_2$ electrode cycled 100 disassembled from $LiCoO_2$/PMM-CPE/Li battery still maintained original

morphology and depicted clearly lattice fringes (corresponding to the (104) facet). Moreover, a compact CEI layer was formed (≈7 nm) using PMM-CPE.

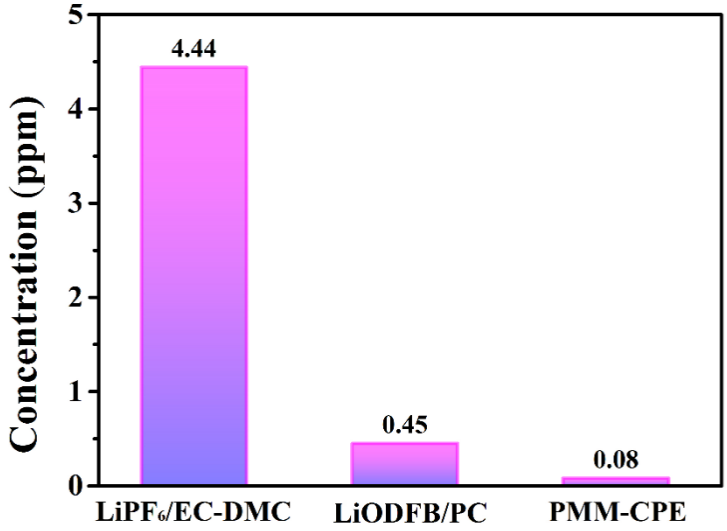

Figure S27. Inductively coupled plasma-optical emission spectrometer (ICP-OES) result of dissolution concentrations of Co ions of cycled $LiCoO_2$ cathode using $LiPF_6$/EC-DMC electrolyte, LiODFB/PC electrolyte and PMM-CPE.

To understand the Co dissolution behavior of cycled $LiCoO_2$ cathodes using $LiPF_6$/EC-DMC electrolyte, LiODFB/PC electrolyte and PMM-CPE, the electrodes were disassembled from cycled $LiCoO_2$ lithium metal battery and soaked the electrode in corresponding solvents (PC or EC-DMC) at 60 °C for 24 hrs (the $LiCoO_2$ lithium metal battery cycled a few rounds and charged to 4.45 V). Obviously, the Co ion content was 0.08 ppm from cycled $LiCoO_2$ cathode disassembled $LiCoO_2$/ PMM-CPE/Li cell, which was much lower than that of liquid electrolyte (LiODFB/PC or $LiPF_6$/EC-DMC), indicated the SEI layer formed by PMM-CPE can alleviate the dissolution of Co ions.

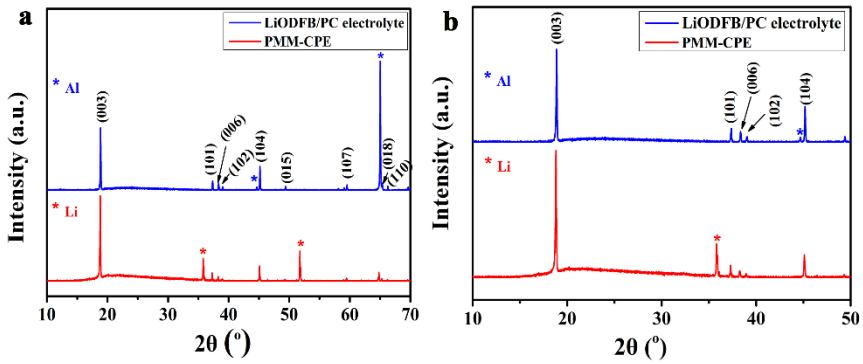

Figure S28. XRD patterns of $LiCoO_2$ electrode using LiODFB/PC electrolyte and PMM-CPE after 100 cycles at 60°C a) ranging from 10-70°, and b) 10-50°.

The phase structure of the $LiCoO_2$ electrodes disassembled from cycled $LiCoO_2$ lithium metal battery using LiODFB/PC electrolyte and PMM-CPE was shown by the XRD patterns in **Figure S28**, all the diffraction peaks can indexed to the α-$NaFeO_2$ structure. According to previous report, the peak intensity ratio of (003)/(104) reflected the integrity and orderliness of layered structure of $LiCoO_2$.[11] It was demonstrated from Figure S28b that $LiCoO_2$ cathode disassembled from cycled $LiCoO_2$/PMM-CPE/Li cell maintained a well layered structure. The peak intensity ratio of (003)/(104) was 5.55, which was larger than that of LiODFB/PC electrolyte (1.34), indicating layerd structure of $LiCoO_2$ cathode employing PMM-CPE was integrity and well-ordered than Li ODFB/PC electrolyte.[12]

References

1. M. Phisalaphong, T. Suwanmajo, P. Sangtherapitikul, *J. Appl. Polym. Sci.* **2008**, *107*, 292.

2. Y. Z. Wan, Y. Huang, C. D. Yuan, S. Raman, Y. Zhu, H. J. Jiang, F. He, C. Gao, *Mat. Sci. Eng. C* **2007**, *27*, 855.

3. H. R. Zhang, Z. Y. Zhao, N. Zhao, Y. Xie, M. Cai, X. Wang, Y. Q. Liu, Z. G. Lan, X. B. Wan, *RSC Adv.* **2017**, *7*, 25009.

4. S. S. Zade, M. Bendikov, *Org. Lett.* **2006**, *8*, 5243.

5. J. C. Chai, Z. H. Liu, J. Ma, J. Wang, X. C. Liu, H. S. Liu, J. J. Zhang, G. L. Cui, L. Q. Chen, *Adv. Sci.* **2017**, *4*, 1600377.

6. S. Matsui, T. Muranaga, H. Higobashi, S. Inoue, T Sakai, *J. Power Sources* **2001,** *97*, 772.

7. B. Xie, Y. J. Mai, J. L. Wang, H. Luo, X. D. Yan, L. Z. Zhang, *Ionics* **2015,** *21*, 909.

8. H. W. Kim, P. Manikandan, Y. J. Lim, J. H. Kim, S. c. Nam, Y. Kim, *J. Mater. Chem. A* **2016,** 4, 17025.

9. X. Y. Qin, J. L. Wang, Y. J. Mai, D. P. Tang, X. Y. Zhao, L. Z. Zhang, *Ionics* **2013,** *19*, 1567.

10. Y. J. Ji, S. G. Li, G. M. Zhong, Z. R. Zhang, Y. X. Li, M. J. McDonald, Y. Yang, *J. Electrochem. Soc.* **2015,** *162*, A7015.

11. N. Wu, Y. Zhang, Y. Guo, S. Liu, H. Liu, H. Wu, *ACS Appl. Mater. Inter.* **2016***, 8*, 2723.

12. D. Luo, G.S. Li, C. Yu, L. S. Yang, J. Zheng, X. F. Guan, L. P. Li, *J. Mater. Chem.* **2012**, *22*, 22233.